ACS Sustainable Chemistry & Engineering

pubs.acs.org/journal/ascecg

Research Article

Integrated Extraction, Enrichment, and Formulation of Parthenolide Using Thermoreversible Aqueous Biphasic Systems toward Antitumoral Applications

Dajana Lazarević, Bojan Kopilovic, Sanja J. Armaković, Stevan Armaković, Bruno M. Baptista, Fani Sousa, Mara G. Freire,* Slobodan B. Gadžurić, and Tatjana Trtić-Petrović*

Cite This: ACS Sustainable Chem. Eng. 2026, 14, 3370−3383

Read Online

ACCESS | Metrics & More | Article Recommendations | Supporting Information

ABSTRACT: This work reports the development of a thermoreversible aqueous biphasic system (ABS) platform for sustainable extraction and enrichment of parthenolide (PAR), a sesquiterpene lactone with anticancer properties, from *Tanacetum parthenium* (feverfew). The ABSs were composed of choline-based ionic liquids (Ch-ILs) and Pluronic 17R4, enabling extraction in a monophasic regime at 25 °C and temperature-triggered phase separation at 35 °C. Binodal curves at the two temperatures were determined for multiple Ch-ILs, revealing that ABS formation efficiency correlates with IL salting-out ability and hydration capacity, with choline dihydrogen phosphate, [Ch][DHP], showing the strongest phase separation and choline lactate, [Ch][Lac], the highest PAR extraction yield. Quantum mechanical and molecular dynamics simulations identified the IL polarity through calculated dipole moments as a key factor for extraction efficiency and supported micelle formation in the Pluronic-rich phase. Optimization via improved mixing raised PAR extraction yields to 3.52 mg/g biomass using ABS composed of [Ch][Lac] and 3.42 mg/g using [Ch][Bit]. To evaluate the sustainability of the developed approach, Path2Green metrics were applied, resulting in a score of 0.363. Dynamic light scattering revealed micelle sizes of 100−200 nm with low polydispersity suitable for drug delivery. Cytotoxicity assays on cancer cell lines confirmed the potent antiproliferative activity of ABS-extracted PAR. The proposed platform integrates extraction, enrichment, and formulation in one step.

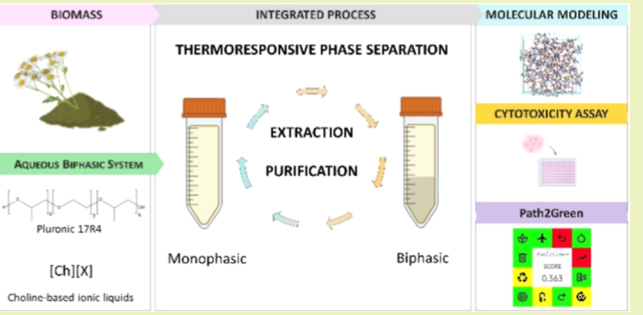

KEYWORDS: *atomistic calculations, green extraction, ionic liquids, parthenolide, Pluronic, thermoreversible aqueous biphasic systems*

Downloaded via UNIV OF AVEIRO 00300 on April 14, 2026 at 16:51:10 (UTC).
See https://pubs.acs.org/sharingguidelines for options on how to legitimately share published articles.

1. INTRODUCTION

Cancer treatment remains a major challenge due to drug resistance, off-target effects, and the complexity of the disease. Despite drug development advancements, a gap persists between the need for effective therapies and the availability of targeted, low-toxicity pharmaceutical compounds.[1] Natural products, particularly plant-derived bioactive compounds, offer promising alternatives, with many phytochemicals demonstrating potent anticancer properties.[2]

Feverfew (*Tanacetum parthenium* (L.) Sch. Bip.) is a medicinal plant known for its active compound, parthenolide (PAR), a sesquiterpene lactone that exhibits anti-inflammatory, anticancer, and neuroprotective effects.[3] In the past decade, there has been a substantial rise in research publications investigating the pharmacological potential of parthenolide, particularly its therapeutic applications.[4] For instance, PAR inhibits nuclear factor-kappa (NF-κB), a key regulator of inflammation, and has shown potential in treating neurodegenerative diseases like Alzheimer's and spinal cord injury disease.[5,6] However, its high cost and limited availability hinder its widespread therapeutic use. Enhancing the extraction efficiency and scalability is therefore essential to making PAR more accessible for pharmaceutical applications.

Traditional extraction methods of PAR from biomass rely on the use of hazardous organic solvents (e.g., methanol, acetonitrile), posing environmental and health risks.[7] Developing more sustainable extraction methods is thus essential to enhancing PAR accessibility while also uncovering potential synergies with other feverfew bioactive compounds. To this end, aqueous solutions of biobased compounds should be the preferred choice over hazardous organic solvents for extracting PAR from biomass. Furthermore, integrated processes incorporating extraction, enrichment, and purification may

Received: October 9, 2025
Revised: December 8, 2025
Accepted: December 9, 2025
Published: December 18, 2025

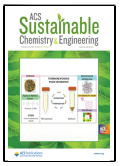

© 2025 American Chemical Society

https://doi.org/10.1021/acssuschemeng.5c10881
ACS Sustainable Chem. Eng. 2026, 14, 3370−3383

Table 1. Chemical Structures, Names, and Abbreviations of the Pluronic, ILs, and Salt Investigated

Name	Abbreviation	Structure	* ω, %	Origin
Choline chloride	[Ch]Cl	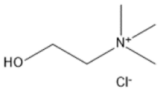	≥98%	Acros Organics
Choline lactate	[Ch][Lac]	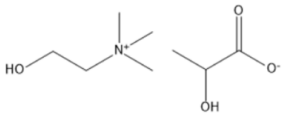	≥98%	Synthesized in this work
Choline bitartrate	[Ch][Bit]	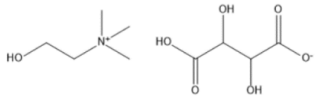	≥97%	Acros Organics
Cholineacetate	[Ch][Ac]	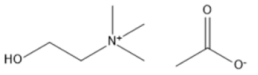	>99%	Iolitec
Cholinetosylate	[Ch][Tos]	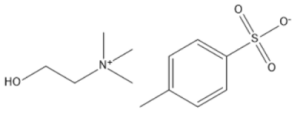	≥98%	Synthesized in this work
Choline dihydrogen citrate	[Ch][DHCit]	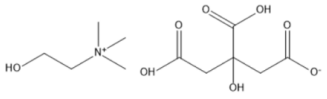	>99%	Sigma Aldrich
Choline dihydrogen phosphate	[Ch][DHP]	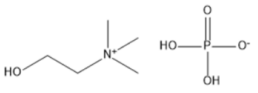	>98%	Iolitec
Pluronic 17R4	PL17R4	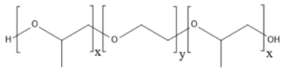	>99%	Sigma Aldrich

[a]Mass fraction purity.

lead to significant economic and environmental benefits. These challenges could be tackled by aqueous biphasic systems (ABS), which are liquid−liquid extraction systems majorly composed of water and two water-soluble components (e.g., polymers, salts, ionic liquids, etc.), in which phase separation occurs above certain concentrations.[8,9] In particular, stimuli-responsive ABS, in which the extraction is carried out in the monophasic regime, whereas the enrichment/separation is further carried out by a biphasic system obtained by an external stimulus, could be considered a smart approach in the development of integrated extraction−enrichment platforms.[10]

Thermoreversible ABS are one type of stimuli-responsive ABS, in which the monophasic to the biphasic regime and vice versa are induced by changes in temperature.[11] Their phase behavior is governed by the critical solution temperature (CST), where phase separation occurs above the upper CST (UCST) or below the lower CST (LCST), being dependent on the ABS components.[11] In addition to conventional components used in ABS formation, such as salts and polymers, there has been a high interest in the ionic liquids (ILs) application in improving the extraction and separation performance of ABS.[12,13] ILs are organic salts with a wide structural diversity, thus allowing for "ideally" designing ILs with the required properties.[14] IL-based ABS can be formed by combining ILs with salts or ILs with polymers, with the latter option being the most appropriate when envisaging the development of thermoreversible ABS. Polymers such as Pluronics, which are thermoresponsive in water, are often applied to form ABS with ILs, thus enabling the formation of thermoreversible ABS. Pluronic polymers, or poloxamers, are amphiphilic triblock copolymers composed of poly(ethylene oxide) (PEO) and poly(propylene oxide) (PPO) blocks, allowing them to self-assemble into micelles, gels, or liquid crystalline phases based on concentration, temperature, and composition.[15] These polymers have shown to be effective in ABS formation with ILs, improving phase separation and enhancing target molecule extraction.[15] Reverse Pluronics (Pluronic-R), with a (PPO)x-(PEO)y-(PPO)x structure, offer unique advantages such as biocompatibility, amphiphilicity, and thermoresponsiveness[16] however, their thermoreversible

https://doi.org/10.1021/acssuschemeng.5c10881
ACS Sustainable Chem. Eng. 2026, 14, 3370−3383

nature has not yet been investigated or exploited. Furthermore, Pluronic-based micelles have gained significant attention as drug delivery systems, but only two Pluronics (F-68 and F-127) have been approved by the FDA and have been extensively used as materials for living bodies.[17] Notably, Deller et al.[18] explored F127 Pluronic micelles loaded with synthetic PAR as a potential treatment for acute lymphoblastic leukemia.

To advance sustainable strategies for PAR isolation, atomistic calculations play a crucial role by offering molecular-level insights into the mechanisms governing extraction efficiency, solubilization, and phase separation. Computational methods such as molecular dynamics (MD) simulations and quantum mechanical calculations may help identify optimal solvent interactions, enhancing the precision and design of green extraction systems.[19,20] By predicting key factors like salting-in and salting-out behaviors, dipole moments, and micelle formation, atomistic modeling bridges the gap between theoretical understanding and experimental optimization.[21,22]

Based on the exposed method, in this work, we demonstrate the development of a sustainable platform to extract and enrich PAR using thermoresponsive ABS composed of Pluronic 17R4 (PL17R4) polymer and choline-based ionic liquids (Ch-ILs). These ABS align with the EU Solvent Emissions Directive.[23] The ABS phase diagrams have been determined at different temperatures to ascertain their thermoreversible behavior and further applied to extract and then enrich PAR from feverfew biomass by applying a temperature stimulus.

The Path2Green metric[24] has been applied to evaluate the sustainability of the extraction. In addition, to characterize the polymeric micelles, in which the PAR is enriched, and better understand the solvent−solute interactions, MD was applied. Finally, the cytotoxicity of the naturally extracted PAR in the Pluronic-rich phases was evaluated on pulmonary, cervical, and prostate cancer cell lines to address its antitumor potential, demonstrating that this platform not only provides high extraction yields from complex biomass but also directly formulates the extracted PAR into bioactive polymeric micelles, effectively bridging sustainable extraction and drug delivery.

2. EXPERIMENTAL SECTION

2.1. Materials. The studied plant sample was the inflorescence of *Tanacetum parthenium* (L.) Sch. Bip., harvested from Novi Sad, Serbia. Voucher specimens (Serbia, Novi Sad, Klisa; Ružica Igić; 2-0014) were confirmed and deposited at the Herbarium BUNS of the University of Novi Sad, at the Department of Biology and Ecology, Faculty of Sciences, Serbia. The sample was air-dried at room temperature with adequate air ventilation. The dried inflorescence was cut into small pieces to facilitate grinding, which was carried out using an electric cutting mill to obtain a fine powder.

The chemical structures, abbreviations, origin, and purity of the investigated ILs are shown in Table 1. Choline bicarbonate, ≥80% in water; lactic acid, ≥85%; and the triblock copolymer PL17R4 with a molar mass of 2700 g mol^{-1} were purchased from Sigma-Aldrich. *p*-Toluenesulfonic acid, ≥98.5%, used for the synthesis of choline tosylate, was purchased from Thermo Scientific.

2.2. Methods. *2.2.1. Synthesis of Ionic Liquids.* All of the ILs, with the exception of choline lactate and choline tosylate, have been commercially acquired. To synthesize choline lactate, choline bicarbonate and lactic acid were mixed in a 1:1.01 molar ratio and stirred for 24 h at room temperature to ensure a complete reaction. Then, a rotary evaporator was used to remove excess volatile solvent. To purify [Ch][Lac], two portions of acetone were added, which dissolved any excess lactic acid and precipitated [Ch][Lac]. Further evaporation using a rotary evaporator was performed to remove the remaining acetone. The IL was vacuum-dried to remove any residual solvent, yielding a light-yellow, viscous liquid. Water content in the IL (≤200 mg dm^{-3}) was determined by Karl Fischer titration. The structure of [Ch][Lac] was confirmed using NMR spectroscopy (Figure S1, in the Supporting Information). Choline bicarbonate and *p*-toluenesulfonic acid were combined in a molar ratio of 1:1.01 and stirred vigorously for 24 h at room temperature to synthesize choline tosylate. After the mixture was stirred, the solvent was removed by rotary evaporation under reduced pressure. Purification was performed by adding two portions of methanol to the dissolved product and mixing thoroughly. Methanol was removed by rotary evaporation under reduced pressure. The IL was dried under a vacuum until a white semisolid material was obtained. Water content in the IL (≤200 mg dm^{-3}) was determined by Karl Fischer titration. The purified and dried choline tosylate was analyzed using NMR spectroscopy (Figure S2, in the Supporting Information).

2.3. Determination of ABS Ternary Phase Diagrams. The binodal curves of the ternary systems composed of the IL + PL17R4 + H_2O were determined by the cloud point titration method at constant temperature, 25 and 35 °C, under atmospheric pressure (p = 0.1 MPa). To keep the temperature constant, a water bath with a temperature precision of ±0.01 °C (ME-18 V Visco-Thermostat, Julabo) was used. Aqueous solutions of each IL were added dropwise to the polymer solution until the solution became turbid (biphasic). Under the same conditions, water was added until the solution became limpid (monophasic). Mass quantification (±10^{-4} g) was used to determine the compositions of the ternary mixtures after adding IL aqueous solution or water.

2.4. Extraction of PAR from Biomass. Figure 1 shows a schematic presentation of the developed integrated extraction−enrichment platform based on the thermoreversible ABS.

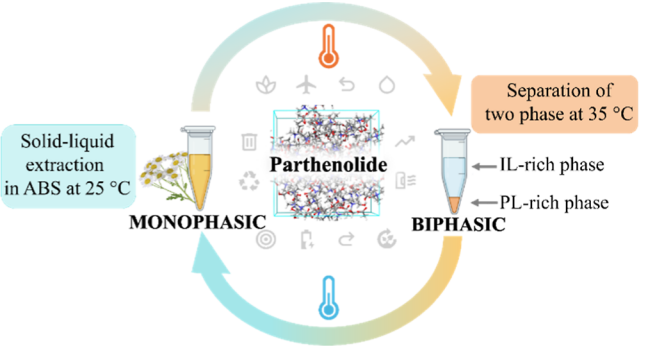

Figure 1. Schematic presentation of the developed integrated extraction−enrichment platform based on the thermoreversible ABS.

Solutions of IL, PL17R4, and water were prepared based on selected extraction points at the monophasic region from the previously determined binodal curves. Dried feverfew powder was mixed with the selected solvent solution in a ratio of 1:50. The samples were placed either in a custom-made vial heating block or in a temperature-controlled shaker platform to ensure the thorough mixing of the biomass and solution. The mixture was stirred at 25 °C for 2 h to maintain a homogeneous, single-phase solution. Then, the liquid phase was separated from the biomass by centrifugation at 25 °C for 5 min at 5000 rpm. The liquid phase was filtered with a nylon filter (0.45 mm) to remove any remaining solid particles. Then, phase separation was promoted by an increase in temperature by carrying out centrifugation of the filtered solutions at 35 °C, for 5 min at 5000 rpm. Finally, the two obtained phases (IL-rich and PL-rich) were separated, diluted, and analyzed by high-performance liquid chromatography (HPLC). The extraction of PAR in the studied ABS systems was expressed through the extraction yield (Y) in mg of PAR per g of dried biomass and partition coefficient (K_{PAR}). The partition coefficient describes the distribution of the extracted

https://doi.org/10.1021/acssuschemeng.5c10881
ACS Sustainable Chem. Eng. 2026, 14, 3370−3383

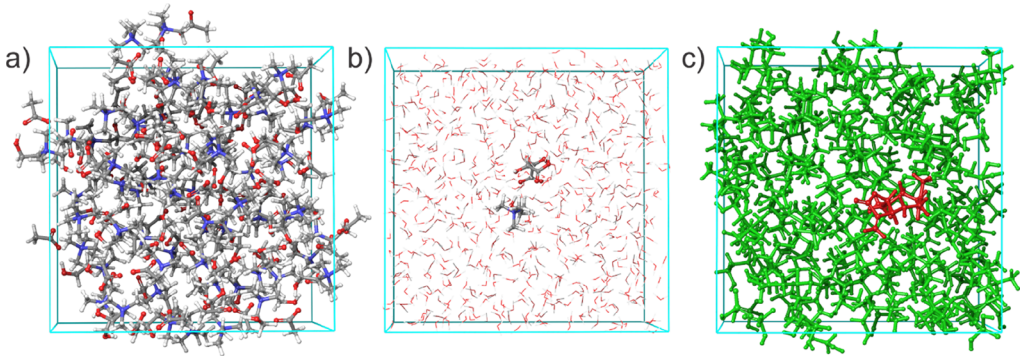

Figure 2. Types of molecular systems used for MD simulations: (a) bulk IL system (64 [Ch][Ac] ion pairs), (b) water-surrounded IL ([Ch][Bit] surrounded by 800 water molecules), and (c) PAR−IL system (PAR, dark-brown molecule, surrounded by 64 [Ch][DHP] ion pairs).

parthenolide between the two phases, and it was calculated as the ratio of the equilibrium concentrations of PAR in the PL-rich phase ($[PAR]_{PL}$) and in the IL-rich phase ($[PAR]_{IL}$). The pH of the IL aqueous solution, ABS monophasic system, and both phases after separation was determined using a Metrohm 827 pH meter (±0.1 uncertainty). The respective results are provided in Table S1, in the Supporting Information. The parthenolide does not suffer speciation under the studied conditions, always being present as a neutral molecule. All experiments in this study were performed in triplicate, and the results are presented as mean values with their corresponding standard deviations.

2.5. Parthenolide Quantification. Parthenolide was quantified using an HPLC system (Shimadzu, model PROMINENCE) equipped with an analytical C18 reversed-phase column (250 × 4.60 mm, Kinetex 5 μm C18 100 Å, purchased from Phenomenex). The mobile phase used consisted of 45% (v/v) of acetonitrile and 55% (v/v) of ultrapure water. The separation was conducted in isocratic mode at a flow rate of 1 mL min^{-1} and using an injection volume of 10 μL. The column oven and the autosampler were operated at a controlled temperature (35 °C). The wavelength was set at 210 nm, and each sample was analyzed at least in duplicate. Calibration curves were established with pure parthenolide dissolved in methanol. Based on the calibration curve, the limits of detection (LOD) and quantification (LOQ) were determined to be 1.51 mg L^{-1} and 4.96 mg L^{-1}, respectively.

The applicability of the HPLC method to real samples was further verified by a spike-and-recovery experiment. First, the HPLC chromatogram of the biomass extract was recorded, followed by analysis of the same extract spiked with a known amount of PAR. The recovery was determined to be 94.3%, indicating that the complex biomass matrix does not cause significant suppression or enhancement of the analytical signal, confirming the reliability of the reported yields. In addition, a comparison of the 3D chromatograms of the PL-rich phase obtained after extraction of synthetic PAR and after extraction from biomass (Figure S3 in the Supporting Information) showed that, at the retention time of 5.9 min, only PAR is present, with no evidence of coeluting compounds.

2.6. Path2Green Metric. The sustainability of the extraction process was assessed using the Path2Green metric,[24] which incorporates 12 principles of green extraction throughout the entire process, from biomass sourcing to waste management. Each principle is evaluated on a scale from −1.00 to +1.00, where higher scores indicate greater alignment with environmentally sustainable methods.

2.7. Dynamic Light Scattering. Dynamic light scattering (DLS) measurements using a Malvern Zetasizer Nano-ZS (Malvern Instruments) were carried out to evaluate the hydrodynamic diameter (dH) of polymeric micelles and their distribution width (PDI, polydispersity index).

2.8. Eukaryotic Cell Culture and Cytotoxicity Assay (MTT). Human lung cancer cells (A549), human prostate cancer cells (LNCaP), and cervical cancer cells (HeLa) were utilized to assess cytotoxicity. The cells were cultured in DMEM-F12 medium supplemented with 10% heat-inactivated FBS and 1% penicillin−streptomycin. Cytotoxicity of the various PAR extracts was evaluated using a Cell Proliferation Kit I (MTT) assay. For this purpose, cells at passages 10−20 were seeded at a density of 1×10^4 cells per well in a 96-well plate. After 24 h, the culture medium was replaced with fresh medium, and the cells were exposed to extracts at specific PAR concentrations, matching reported PAR ranges.[25] Also, the Pluronic control was prepared using the same dilution factor as that in the extracts. The MTT assay was conducted for 48 h. The medium was then replaced with a mixture of 100 μL of medium and 10 μL of MTT reagent, followed by a 4 h incubation at 37 °C in a humidified atmosphere with 5% CO_2. After incubation, the medium was removed, 100 μL of dimethyl sulfoxide (DMSO) was added to each well, and the plate was agitated for approximately 15 min to solubilize the crystals. Absorbance was measured at 570 nm by using a microplate reader. All experiments were performed in triplicate. For a positive control, cells were treated with 70% ethanol. Cytotoxicity tests were repeated three times with independent culture preparations. The results are presented as the mean ± standard error.

2.9. Computational Studies. All molecular structures studied in this work have been preoptimized using the semiempirical GFN2[26,27] level of theory using the online molecular modeling platform atomistica.online, freely available at https://atomistica.online.[28,29] Optimized molecular structures were further subjected to global geometry optimization and ensemble generator (GOAT)[30,31] calculations using the GFN2 method to identify the global minimum structures. Global minimum structures were reoptimized using the density functional theory approach with the r2SCAN-3c[32] method. Frequency calculations were performed to ensure that the true ground states have been identified. All DFT calculations have been performed with the ORCA modeling package.[32−40] All input files for the ORCA calculations have been generated using the online ORCA input generator tools (for single and batch input files) of the atomistica.online platform. MD simulations were performed using the Desmond[41,42] program of the Schrödinger Materials Science Suite 2022-3. The OPLS3e force field[43−47] was used in combination with a 9 Å cut off and a temperature of 300 K. The obtained optimized structures of the ILs are presented in Figure S4 in the Supporting Information.

Based on the r2SCAN-3c calculations, a set of key molecular descriptors and energetic parameters were obtained. Among these, the ion pair binding energies (IPBE) and dipole moments emerged as being the most significant. r2SCAN-3c-optimized structures were used to build the three types of molecular systems used for MD simulations (Figure 2). The first type of MD system, Figure 2a, represents the bulk IL phase, composed solely of ionic liquids, with 64 cation−anion pairs for each studied IL. This system was used to calculate the solubility parameter (δ), a key measure for evaluating miscibility between components. The second type of MD system, Figure 2b, is the IL−water system, consisting of a single cation−anion pair surrounded by approximately 800 water molecules. This system was used to assess the anion−water interaction strength, a critical

https://doi.org/10.1021/acssuschemeng.5c10881
ACS Sustainable Chem. Eng. 2026, 14, 3370−3383

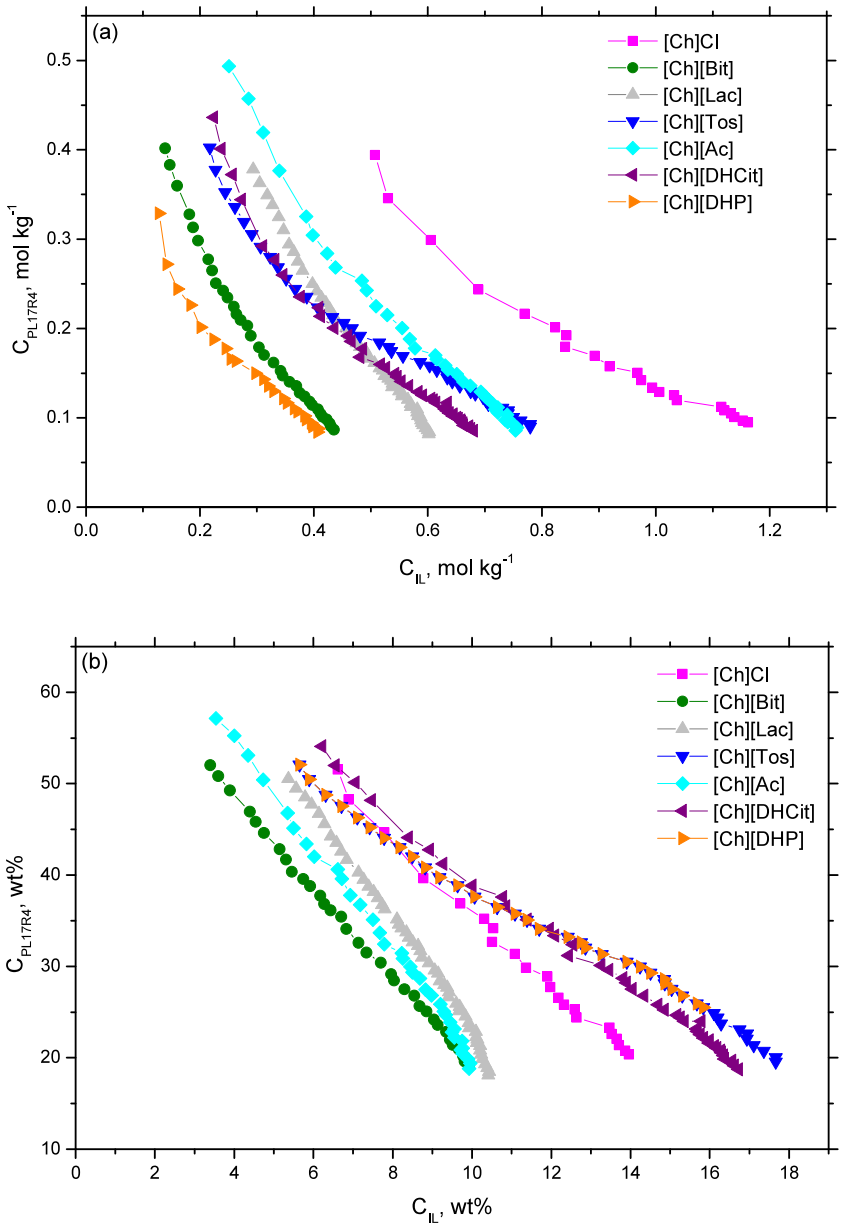

Figure 3. Phase diagrams of the studied {ILs + PL17R4 + H_2O} at T = 25 °C and atmospheric pressure (p = 0.1 MPa), presented in mol kg^{-1} (a) and in weight fraction (b). Water content is not shown.

factor in determining anion hydration capacity, which is an essential parameter influencing the efficiency of ILs in ABS formation. Finally, the third type of MD system, Figure 2c, consists of 64 IL ion pairs and a single PAR molecule. This system was designed to calculate interaction energies between PAR and ILs, providing insights into the strength of their interactions and their role in PAR solubilization and partitioning to the opposite ABS phase.

3. RESULTS AND DISCUSSION

3.1. Thermoreversible ABS Phase Diagrams. The initial stage of this work involved determining the ABS binodal curves at two temperatures by using various biocompatible choline-based ILs (Ch-IL) and a thermoreversible polymer. These data are essential for identifying the monophasic and biphasic regimes and the mixture compositions at which the thermoreversible systems could be applied. To investigate the effect of ILs on ABS formation and parthenolide extraction, seven Ch-ILs were studied. The binodal data for {Ch-IL + PL + H_2O} determined at 25 and 35 °C under atmospheric pressure are given in the Supporting Information (Tables S2 and S3). In each system, the top phase corresponds to the IL-rich phase, while the bottom phase is PL-rich. Figure 3a,b shows the ABS phase diagrams at a constant temperature (25 °C) in molality units and in weight fraction. Molality (mol·kg^{-1}) of the ILs, as one of the temperature-independent concentration units, was used to address the IL's ability to undergo liquid−liquid demixing. A smaller area below the binodal curve indicates a higher ABS formation ability. Accordingly, and since all ILs share the same cation, the IL anions' ability to form ABS at a fixed amount of PL17R4 (0.2 mol kg^{-1}) follows the order: $[DHP]^-$ < $[Bit]^-$ < $[Tos]^-$ < $[Lac]^-$ < $[DHCit]^-$ < $[Ac]^-$ < Cl^-. The salting-out effect and interactions among IL anions, PL, and water molecules play a key role in ABS formation when ILs and a more hydrophobic PL are combined. As experimentally shown, due to its strong hydration capacity and potential to promote polymer

https://doi.org/10.1021/acssuschemeng.5c10881
ACS Sustainable Chem. Eng. 2026, 14, 3370−3383

dehydration, the IL containing $[DHP]^-$ is the most efficient salting-out agent. On the other hand, [Ch]Cl is the weakest salting-out agent investigated.

To validate the observed salting-out effects of the different IL anions and respective ability to form ABS, the solubility parameter (δ) was calculated for ILs, polymer, and PAR, with the difference in this parameter ($\Delta\delta$) relative to either PL17R4 or PAR used as an indicator of mutual compatibility, whose results are shown in Table 2. A lower $\Delta\delta$ between the two components suggests higher compatibility and miscibility.

Table 2. Solubility Parameters and Their Differences, Determined by MD Simulations

	δ [MPa$^{1/2}$]	$\Delta\delta$ IL vs PL [MPa$^{1/2}$]	$\Delta\delta$IL vs. PAR [MPa$^{1/2}$]	anion−water interaction ($E_{int}^{(a-w)}$) [kcal/mol]	IPBE [kcal/mol]
			salt		
[Ch]Cl	55.57	34.61	35.75	−137.70	−104.01
			ILs		
[Ch][Bit]	49.83	28.87	30.02	−157.90	−96.90
[Ch][Lac]	49.51	28.55	29.70	−149.34	−101.88
[Ch][Tos]	43.60	22.64	23.79	−149.85	−98.17
[Ch][Ac]	54.58	33.62	34.77	−160.12	−111.18
[Ch][DHCit]	44.61	23.65	24.79	−142.59	−95.80
[Ch][DHP]	55.34	34.38	35.52	−154.85	−105.14
			polymer		
PL17R4	20.96	0.00	1.15	N/A	N/A
			natural extracted compound		
PAR	19.81	N/A	0.00	N/A	N/A

Experimental results have identified [Ch][DHP] as the most efficient IL for ABS formation. Indeed, $\Delta\delta$ for $[DHP]^-$ is among the highest of all calculated values, clearly indicating its low miscibility with PL17R4. However, the δ values also suggest that the choline salt with Cl^- has the highest $\Delta\delta$ against PL17R4, implying that [Ch]Cl should be the most effective for building ABS. However, this contradicts the experimental findings. This discrepancy suggests that solely relying on solubility parameters between the IL and the polymer, or addressing their mutual incompatibility, is not enough, demonstrating that ABS formation is a more complex process influenced by multiple factors. Since water is also present, one such factor is the ions' hydration capacity, which plays a crucial role in determining the efficiency of ILs in phase separation.

To properly assess the hydration capacity of anions, we refer to the results of MD simulations performed on a system consisting of a single ion pair surrounded by water molecules. From these simulations, we calculated the interaction energy between the anion and surrounding water molecules ($E_{int}^{(a-w)}$). The data in Table 2 reveal a significant difference in the $E_{int}^{(a-w)}$ between $[DHP]^-$ and Cl^-. Specifically, $[DHP]^-$ interacts more strongly with water ($E_{int}^{(a-w)}$ = −154.84 kcal/mol) compared to Cl^- ($E_{int}^{(a-w)}$ = −137.70 kcal/mol). This explains why the IL containing $[DHP]^-$ is a stronger salting-out species. Its strong interactions with water molecules draw them out of the polymer phase, enabling phase separation. In contrast, [Ch]Cl shows the weakest hydration capacity among all of the studied anions, making it less effective at dehydrating the polymer phase. This explains its poor performance in ABS formation compared to $[DHP]^-$.

The efficiency of an IL as a salting-out agent in ABS is thus governed by a delicate balance between the inherent hydration capacity of its anion and the strength of the cation−anion interaction (ion pair binding energy, IPBE). A high anion−water interaction energy is a prerequisite for strong salting-out, but its effectiveness is contingent upon the anion's ability to freely interact with the water network. If the anion is tightly bound to the cation (high IPBE), then its hydration is sterically and electrostatically hindered, diminishing its overall capacity to compete for water molecules and dehydrate the polymer. This interplay provides a more holistic framework for understanding the phase behavior.

Another discrepancy found arises in the case of [Ch][Ac], which exhibits a very high $\Delta\delta$ parameter and the most negative $E_{int}^{(a-w)}$, suggesting that $[Ac]^-$ has the strongest hydration capacity and should be the most effective IL for salting-out the polymer in aqueous solution. However, experimental results indicate that the salting-out property of [Ch][Ac] is relatively poor compared to those of other ILs. This inconsistency can be explained by the IPBE, which is the strongest in the case of [Ch][Ac]. A higher IPBE value means that the $[Ac]^-$ anion remains tightly associated with the cation, limiting its ability to interact freely with water molecules. As a result, despite the high hydration capacity of $[Ac]^-$, its strong ion pairing restricts its effectiveness in being hydrated and promoting ABS formation. This analysis confirms that a high IPBE can effectively "lock" an anion with high intrinsic hydration capacity, making it a poor salting-out agent, whereas an anion with a moderately high $E_{int}^{(a-w)}$ and a lower IPBE is more freely available to interact with water and is therefore a more efficient promoter of phase separation.

Results suggest that low IL concentration (7−10 wt %) can be used to prepare ABS for the extraction of PAR at 25 °C (Figure 3b). Still, to harness the potential of thermoreversible ABS for extraction, we also determined binodal curves at 35 °C. Figure 4a,b illustrates the binodal curves for {IL + PL17R4 + H_2O}, for the [Ch][Lac] and [Ch][Bit] at two temperatures (25 and 35 °C). Remaining phase diagrams and experimental data are given in Figure S4 and Table S3 in the Supporting Information. Since this study compares the same ABS at two different temperatures, envisaging extraction purposes, the results are now presented as weight percentages. All systems show an LCST behavior, maintaining a monophasic system at lower temperatures, while phase separation occurs at higher temperatures. The temperature of 25 °C was selected for its proximity to room temperature, while 35 °C was chosen to ensure the stability of the target bioactive compound. Furthermore, the studied thermoreversible ABS composed of IL and Pluronic will enable separation without additional chemicals or energy-intensive steps. Based on the region between the two solubility curves, in which the thermoreversible behavior can be applied, the extraction points were selected so that, in all cases except for [Ch][Tos], the concentration of PL17R4 remains constant while the concentration of IL depends on its ability to form an ABS. The extraction points were selected between the ternary phase diagrams at 25 and 35 °C, allowing for extraction in the monophasic region (25 °C) and phase separation at 35 °C (Figures 4a,b and S5 in the Supporting Information).

3.2. Thermoreversible ABS for the Integrated Extraction and Enrichment of PAR. While the partitioning

https://doi.org/10.1021/acssuschemeng.5c10881
ACS Sustainable Chem. Eng. 2026, 14, 3370−3383

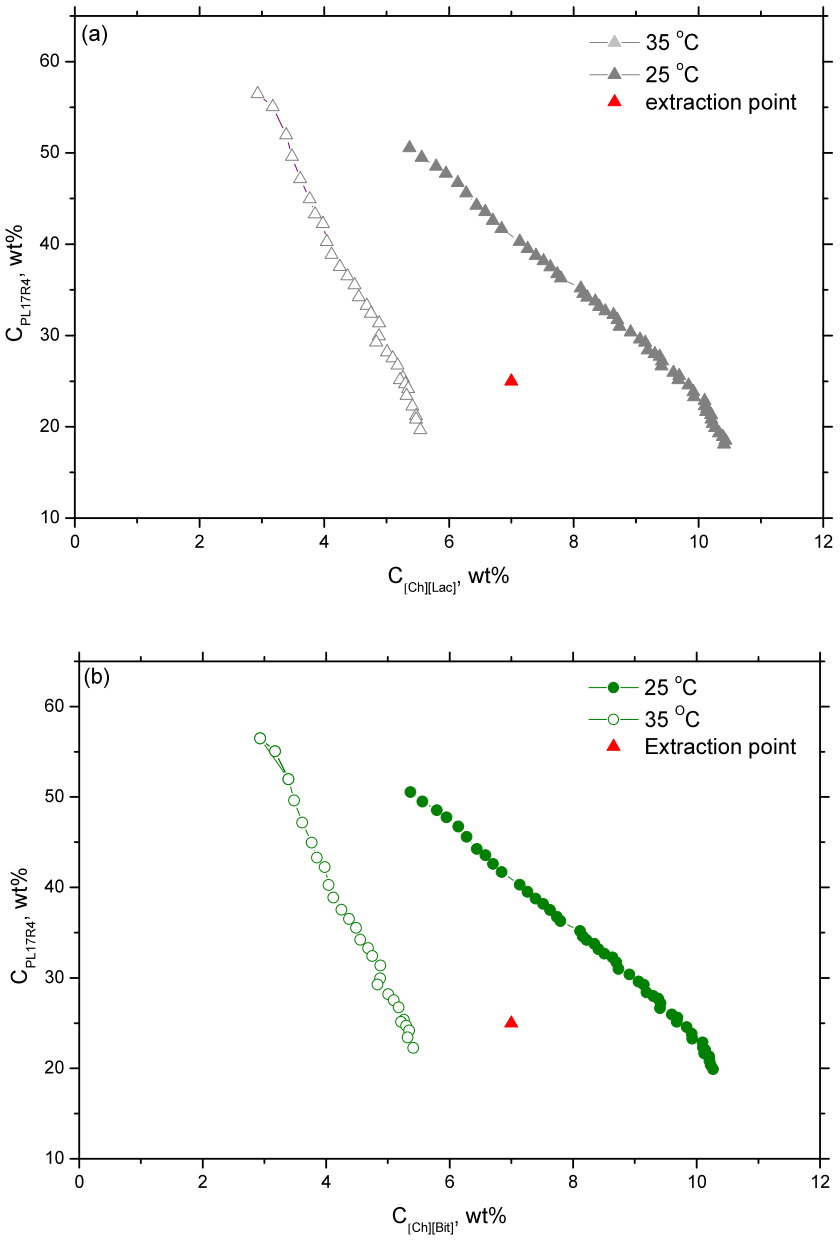

Figure 4. Phase diagrams at 25 and 35 °C with selected extraction points for systems composed of (a) {[Ch][Lac] + PL17R4 + H_2O} and (b) {[Ch][Bit] + PL17R4 + H_2O}.

behavior of pure, synthetic PAR in ABS has been previously investigated,[48] extraction from a complex biomass matrix presents additional challenges. Feverfew contains a diverse array of secondary metabolites, including other sesquiterpene lactones and flavonoids.[3] The presence of these coextracted compounds can compete for solvation, potentially influencing the extraction efficiency of the target molecule (PAR) and its subsequent partitioning between the ABS phases. Therefore, a key aspect of developing a successful integrated process is ensuring its selectivity and robustness within the complex chemical environment.

A solid−liquid extraction was employed to isolate parthenolide from biomass using the studied thermoreversible ABS {IL + PL17R4 + H_2O}, enabling the efficient separation of the target compound through a temperature-induced phase transition. The extraction systems consisted of 25 wt % of PL17R4 (except 35% for [Ch][Tos]), varying the concentration of the IL in the range from 7 to 10 wt % (Figures 4a,b andS5 in the Supporting Information). Under these conditions at 25 °C, the extraction occurred in a monophasic region, where both the IL and polymer were present (Figure 1). Biomass was separated by centrifugation at 25 °C. Then, centrifugation of the obtained liquid phase at 35 °C led to phase separation, resulting in an IL-rich phase and a PL-rich phase, with the latter containing enriched PAR in the form of micelles.

First, the effect of the solid-to-liquid phase ratio, the amount of biomass to the amount of solvent, was examined at 1:10 and 1:50. At a 1:50 phase ratio, the separation of the phases after extraction is easily achievable, resulting in distinctly separated PL-rich and IL-rich phases. In contrast, at a 1:10 ratio, the two phases cannot be effectively separated, and during the formation of the two phases at 35 °C, the volume of the PL-rich phase is exceptionally small. Therefore, in all further

https://doi.org/10.1021/acssuschemeng.5c10881
ACS Sustainable Chem. Eng. 2026, 14, 3370−3383

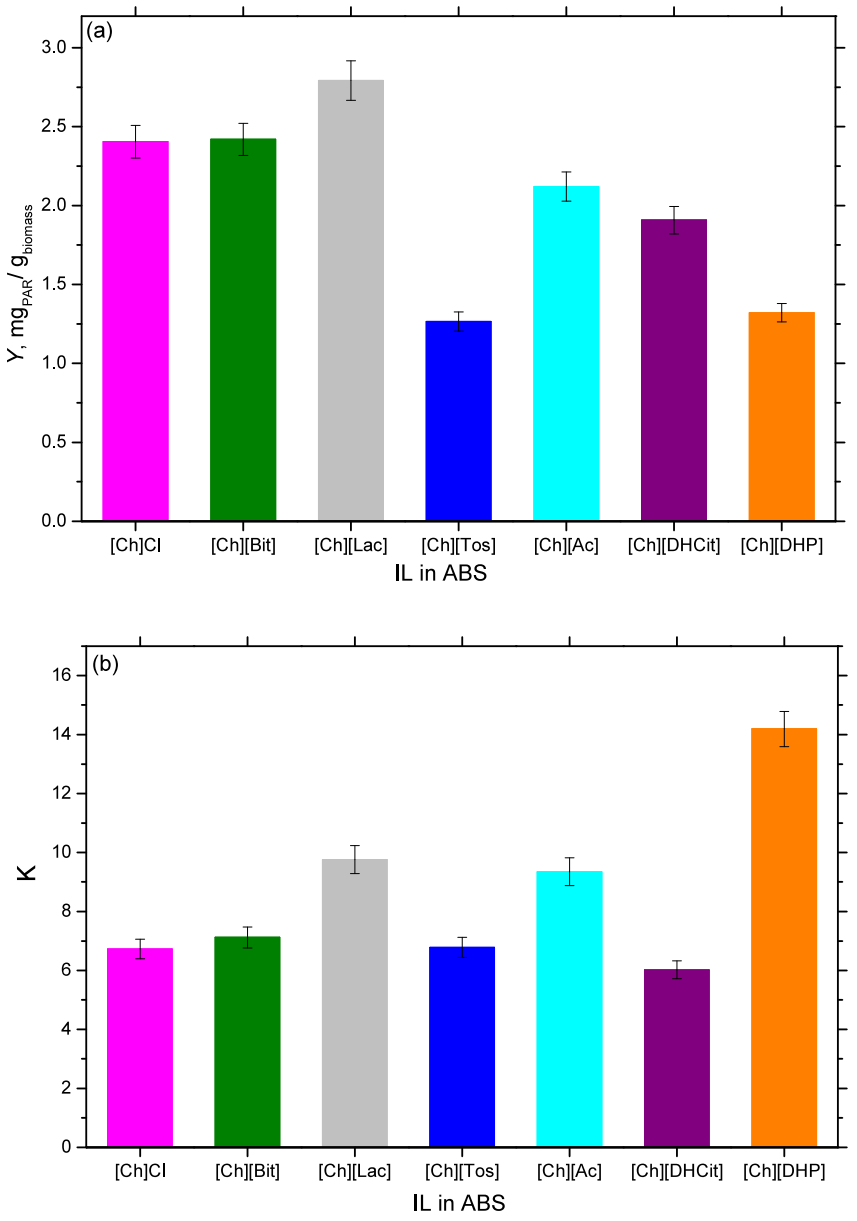

Figure 5. (a) Extraction yield of PAR (Y) in the monophasic region obtained at 25 °C and (b) partition coefficient (K) obtained in the biphasic regime at 35 °C.

experiments, the solid-to-liquid phase ratio was kept constant at 1:50.

The results of PAR extraction−extraction yield (Y, $mg_{PAR}/g_{biomass}$) in the monophasic region obtained at 25 °C and partition coefficient (K) obtained in the biphasic regime at 35 °C are shown in Figure 5a,b, demonstrating a distinct preferential migration of PAR to the PL-rich phase. The detailed results of PAR extraction are provided in Table S4 in the Supporting Information.

The high extraction yields (Figure 5a) and preferential partitioning of PAR to the PL-rich phase ($K > 1$, Figure 5b) can be attributed to its distinct hydrophobicity (log $P = 2.3$),[49] which aligns with our previous work on synthetic PAR.[48] This behavior is further supported by the computational data in Table 2, which shows a low $\Delta\delta$ between PL17R4 and PAR, indicating high compatibility, and a significantly higher $\Delta\delta$ between all ILs and PAR, confirming their lower miscibility. Notably, these results were achieved using feverfew biomass, demonstrating the method's robustness in a complex matrix. The process also exhibits inherent selectivity: highly polar coextractives (e.g., sugars, organic acids) are expected to remain in the hydrophilic IL-rich phase, while the hydrophobic core of the PL-micelles provides a specific solubilization environment that favors the encapsulation of hydrophobic compounds including PAR, which is the most abundant sesquiterpene lactone in *Tanacetum parthenium*. This high enrichment of PAR, combined with specific HPLC quantification, ensures the reported yields accurately reflect the target compound's extraction. Furthermore, the potent bioactivity of the final PL-rich phase (Section 3.4) indicates that any copartitioned compounds do not hinder, and may even synergistically enhance, the desired biological effect.

The highest extraction yield ($Y = 2.79$ $mg_{PAR}/g_{biomass}$) of PAR from biomass was achieved by employing the system {[Ch][Lac] + PL17R4 + H_2O}, which further leads to a partition coefficient of 9.76 after phase separation and ABS

https://doi.org/10.1021/acssuschemeng.5c10881
ACS Sustainable Chem. Eng. 2026, 14, 3370−3383

formation. Approximately 15% lower yield of PAR was obtained with the systems {[Ch][Bit] + PL17R4 + H_2O} (Y = 2.42 $mg_{PAR}/g_{biomass}$) and {[ChCl + PL17R4 + H_2O} (Y = 2.40 $mg_{PAR}/g_{biomass}$), leading to a partition coefficient of 7.12 and 6.73, respectively. The structural similarity between [Ch][Lac] and [Ch][Bit], particularly a high density of polar functional groups, is hypothesized here to contribute to their similarity and high PAR extraction efficiency. The system composed of {[Ch]Cl + PL17R4 + H_2O} is also promising for the extraction of PAR; however, the previously shown solubility curves (Figure 3) indicate that a higher concentration of [Ch]Cl is required to achieve biphasic separation compared to [Ch][Lac] and [Ch][Bit]. Accordingly, [Ch]Cl was excluded from further optimization. In particular, [Ch]-[DHP] has the best partitioning coefficient, meaning that the respective ABS is relevant for enrichment purposes, but it also extracts the second-lowest quantity of PAR. The extraction yields of PAR in the systems with [Ch][Ac] and [Ch][DHCit] are between those obtained for [Ch][DHP] and [Ch][Tos], and the best systems are identified. With the exception of [Ch][Tos], the values provided in Table 2 indicate that the $\Delta\delta$ between [Ch][Lac] or [Ch][Bit] and PAR is among the lower ones, meaning that the miscibility of PAR in these two ILs is higher, further corroborating the higher extraction yield obtained with them. Accordingly, the highest between ILs and PAR was observed for the IL [Ch][DHP], the respective system being the one with the lowest extraction yield. Nevertheless, not all trends in extraction yield correlate with the relationship between ILs and PAR.

The dependence of the PAR extraction efficiency on ILs has been further investigated using computational results. It was found that the dipole moment of ILs plays a key role in determining the extraction efficiency. The calculated IL dipole moments and the corresponding extraction yields of PAR are summarized in Table 3.

Table 3. IL Dipole Moment (D) and Yield of PAR (Y)

IL	dipole moment [D]	Y [$mg_{PAR}/g_{biomass}$]
[Ch]Cl	12.48	2.40
[Ch][Bit]	9.24	2.42
[Ch][Lac]	12.87	2.79
[Ch][Tos]	9.52	1.26
[Ch][Ac]	10.04	2.12
[Ch][DHCit]	10.31	1.91
[Ch][DHP]	9.41	1.32

From the data shown in Table 3, there is a strong correlation between higher dipole moments and increased PAR extraction efficiency. ILs with higher values of dipole moments ([Ch]Cl, [Ch][Lac], and [Ch][Bit]) demonstrate enhanced PAR extraction, likely due to stronger solvation. In contrast, ILs with lower dipole moments ([Ch][Tos] and [Ch][DHP]) exhibit a reduced extraction yield, suggesting weaker molecular interactions with PAR. These computational findings align with experimental results, where extracted PAR amounts ranged from 1.26 to 2.79 mg/g biomass. The found linear correlation (r = 0.75, p = 0.05) suggests a statistically significant relationship between dipole moment and the extraction of PAR, indicating that ILs with higher dipole moments may favor more efficient extraction. This strong trend, despite the complexity of the biomass matrix, underscores the potential of the dipole moment as a predictive descriptor for extraction efficiency, warranting further investigation with a broader set of ILs. Essentially, the regression model predicts that for every 1 D increase in dipole moment, the extracted mg of PAR increases by approximately 0.24 mg. This supports the model in which the ILs with higher dipole moments enhance PAR solubilization, leading to improved extraction efficiency. Although the p-value is slightly above the conventional threshold of statistical significance, it strongly suggests a meaningful trend that warrants further investigation with a larger data set.

The extraction process was further optimized by using the ionic liquids [Ch][Lac] and [Ch][Bit], which exhibited the highest extraction yield. Effective mixing is crucial in a solid–liquid extraction system as it increases the contact surface area between the solid and liquid phases. Initially, PAR was extracted from feverfew biomass using a custom-made vial heating block with agitation provided by a magnetic mixing plate. To improve the extraction efficiency, a temperature-controlled shaker platform was introduced, ensuring more uniform and rigorous mixing. Other extraction conditions, including the solid-to-liquid ratio, temperature, and extraction time, remained unchanged. Shaking was adopted as an alternative to conventional mixing methods due to its advantages in promoting better mass transfer, reducing channeling effects, and ensuring more uniform extraction. After optimization, the extraction yield for [Ch][Lac] increased from 2.79 to 3.52 mg/g of biomass, while for [Ch][Bit], it improved from 2.42 to 3.42 mg/g. Compared to literature-reported methods using acetonitrile as a reference solvent, our optimized approach using aqueous solutions of Pluronic and the ILs [Ch][Lac] and [Ch][Bit] achieved comparable parthenolide yields.[7] We further highlighted the practical and environmental advantages of the proposed extraction method. Unlike conventional methods, we avoid the use of harmful solvents, in accordance with green chemistry principles. Despite advanced methods, such as supercritical fluid extraction, our approach operates under ambient or mild conditions, avoiding the requirement for high temperatures and pressures. This makes it substantially more energy efficient and accessible while retaining a good extraction performance.

The extraction yields reported here, reaching up to 3.52 mg/g, are particularly significant as they were achieved using dried and powdered feverfew inflorescence, a real and complex plant material. This demonstrates the robustness of the thermoreversible ABS platform, which successfully operates despite the presence of a diverse matrix of coextractives like polysaccharides, proteins, and other phytochemicals. The success of this system with feverfew biomass underscores its potential for broader application. The mechanism driving the extraction and enrichment—partitioning based on hydrophobicity and encapsulation into Pluronic micelles—is not unique to PAR. Therefore, this platform could be readily adapted for the integrated extraction and formulation of other medium-to-high log P bioactive compounds from various plant sources. For instance, similar sesquiterpene lactones (e.g., artemisinin), flavonoids (e.g., quercetin), or cannabinoids could be targeted using the same ABS principles, potentially by tailoring the hydrophobicity of the IL and/or polymer to the specific solute of interest.

To further validate the development of a more sustainable approach, the proposed thermoreversible ABS for PAR extraction from biomass was evaluated using the Path2Green framework,[24] assessing sustainability across 12 principles

https://doi.org/10.1021/acssuschemeng.5c10881
ACS Sustainable Chem. Eng. 2026, 14, 3370−3383

(Figure 6). Key findings can be summarized as follows: Biomass (+0.75)—feverfew biomass is naturally derived.

Figure 6. Path2Green score and pictogram of each principle.

Although feverfew can be locally sourced, maximizing accessibility and minimizing resource inputs and logistics impacts in line with principle 2 (transfer), we used biomass from a location requiring transport over 80 km. Pretreatment (−0.2)—a minor drawback due to manual crushing. Solvents (+1)—a major advantage, as the system uses low-toxic solvents[50] instead of conventional hazardous alternatives like methanol and acetonitrile. Scaling (−1)—batch processing limits scalability; transitioning to continuous flow will enhance efficiency; Purification (+1)—direct extract application (as shown in the next section) eliminates additional purification steps; Yield (0)—maximum extraction of targeted biocompounds (PAR). Post-treatment (+1)—extracts do not require further processing. Energy (0)—low energy demand but currently reliant on heating from nonrenewable sources; integrating renewable energy remains a future goal. Application (+0.5)—pharmaceutical (anticancer, migraine treatment),[3−6] antioxidant,[51] and nutritional (functional food)[52,53] applications are supported by cell line testing (shown in the next sections) and literature; Repurposing (0)—no closed-loop solutions explored yet. Waste Management (0)—the ionic

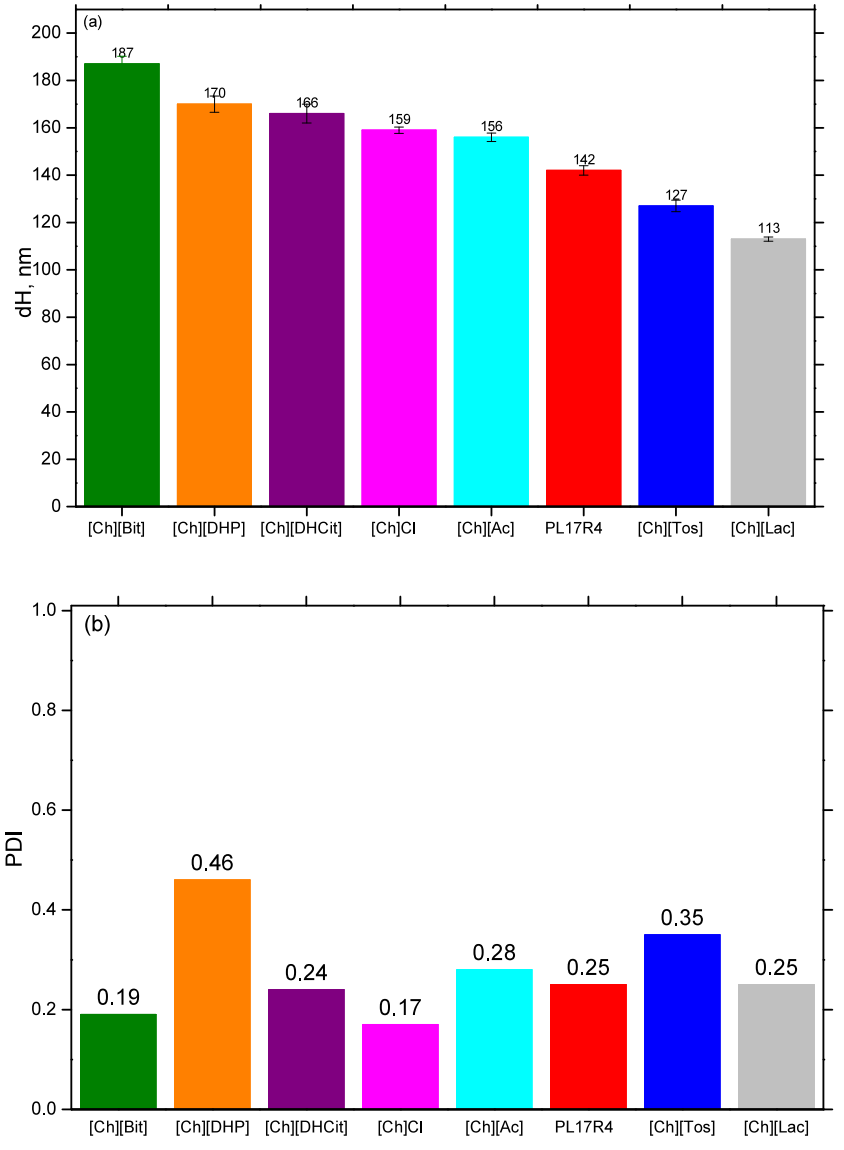

Figure 7. (a) Hydrodynamic diameter at 25 °C of the PL-rich phase and of an aqueous solution of pure Pluronic 17R4; (b) polydispersity index.

https://doi.org/10.1021/acssuschemeng.5c10881
ACS Sustainable Chem. Eng. 2026, 14, 3370−3383

liquid solvent is reusable, and the remaining biomass is nontoxic and can be used as fertilizer, for instance. According to these, a final score of 0.363 was obtained for the developed process, indicating that the proposed integrated PAR extraction and enrichment is moderately sustainable, having room for improvement. Parameters like scalability (−1), pretreatment (−0.2), and energy dependency (0) need to be improved. Future improvements, such as transitioning to continuous processing, integrating renewable energy, and developing closed-loop solutions, could push the score closer to +1, making the process even greener. In summary, according to the Path2Green metrics, a 0.363 score reflects a promising yet improvable sustainable approach, already greener than conventional methods but with opportunities for further refinement.

3.3. Characterization of PAR−Polymeric Micelles. As described above, after the two-phase separation through ABS, PAR is enriched in the polymer-rich phase in the form of micelles. Nevertheless, the micelle size is a critical factor influencing the behavior, efficacy, and safety of drug-loaded micellar delivery systems. Understanding its relationship with drug properties is essential for optimizing drug delivery. DLS was used to determine the micelle size in solution, where the dH represents the diameter of a sphere diffusing at the same rate as the molecule of interest. A lower PDI indicates a more uniform micelle population, making it a key parameter in the DLS analysis.

After the PAR extraction and ABS formation by increasing the temperature up to 35 °C, the PL-rich phase was separated from the IL-rich phase, diluted with ultrapure water, and analyzed using DLS. A 1% PL17R4 solution was used as the control for comparison. As shown in Figure 7a, the presence of different ILs either increased or decreased the micelle size compared to the ones obtained in aqueous solutions of pure PL17R4. The micelle sizes ranged from 100 to 200 nm, indicating well-defined nanoscale structures, while the PDI values varied between 0.17 and 0.46, reflecting some size variability (Figure 7b). Since PDI values below 0.5 indicate a relatively uniform size distribution, the micelles obtained in this study via the integrated approach showed good homogeneity.

From a clinical perspective, various long-circulating, small-sized (100−200 nm) microparticulate drug carriers have demonstrated effective accumulation in tumors via the enhanced permeability and retention effect,[54] supporting the adequacy of our micelle sizes for such a purpose. A study on nanoparticle permeation and retention properties across different sizes revealed that 60% of nanoparticles within the 100−200 nm range persisted longer in plasma, compared to only 20% of nanoparticles smaller than 50 nm and 20% of nanoparticles larger than 250 nm. Additionally, another study found that nanoparticles in the 100−200 nm range exhibited four times greater absorption compared to those smaller than 50 nm or larger than 300 nm.[55]

The interaction strengths between PAR and ILs, E_{int}^{PAR-IL}, were investigated by MD, as summarized in Table 4. In addition to having PAR in the polymer-rich phase, there is also IL present in a lower amount in this phase. The obtained results show that the interaction strength between PAR and ILs influences micelle size.

Molecular dynamics simulations indicate that ILs with stronger ([Ch][DHP], [Ch]Cl, and [Ch][Bit]) lead to larger micelles due to enhanced hydrophobic stabilization. In contrast, ILs with weaker interactions ([Ch][Tos] and [Ch][Lac]) result in smaller micelles due to reduced stabilization and a weaker tendency for PAR encapsulation. Furthermore, regression analysis confirmed a significant negative correlation ($r = -0.85$, $p = 0.02$) between the interaction energy of IL-PAR and micelle size, indicating that stronger PAR−IL interactions favor larger micelles. Essentially, the regression model predicts that for every 1 kcal/mol increase in binding strength, the micelle size increases by approximately 9 nm. The obtained regression results support the approach in which ILs with stronger interactions enhance hydrophobic stabilization and promote micelle growth.

Table 4. PAR−IL Interaction Energies and Micelle Sizes

IL	E_{int}^{PAR-IL}/[kcal/mol]	dH/nm
[Ch][Ac]	−51.263	156 ± 1.75
[Ch][Bit]	−52.703	187 ± 3.20
[Ch]Cl	−53.745	159 ± 1.33
[Ch][DHP]	−53.924	170 ± 3.49
[Ch][DHCit]	−52.407	166 ± 3.98
[Ch][Lac]	−48.782	113 ± 0.91
[Ch][Tos]	−47.763	127 ± 2.43

3.4. Cytotoxicity of ABS-Extracted Formulations. Envisaging the final application of the extracted PAR toward cancer treatment, the cytotoxicity of both the extracts and the ABS components was investigated. A colorimetric MTT assay was performed to evaluate cell viability in HeLa (cervical), A549 (lung), and LNCaP (prostate) cancer cells (Figure 8a−c). Tested compounds included [Ch]Cl, [Ch][Lac], [Ch]-[Bit], PL17R4, PAR, and PAR-containing PL-rich phases (extracts) from the best-performing ABS. Extracts were diluted to match reported PAR concentrations (0.005, 0.025, and 0.05 mM).[25]

After 48 h of incubation, the selected ILs were noncytotoxic at 0.1 and 1 mM, confirming their suitability as extraction and formulation components. PAR-containing extracts significantly reduced cancer cell viability at 0.005 and 0.025 mM, with stronger effects than pure PAR. At 0.05 mM, cytotoxicity levels became comparable across PAR, Pluronic, and extract-treated cells, likely due to the high inherent toxicity of Pluronic (at 6.095 mM) masking PAR's specific effects.

These findings align with previous reports showing that PAR exhibits potent antiproliferative effects on cancer cell lines in a concentration- and time-dependent manner. For example, synthetic PAR inhibited the proliferation of A549 lung cancer cells and reduced Ki67 and PCNA expression after 24−48 h at 10 μM.[25] Similar concentration-dependent growth inhibition has been reported in breast cancer cells (MDA-MB-231), with IC_{50} values between 0.01228 mM and 0.02544 mM depending on the tested PAR derivative,[56] and in rheumatoid arthritis fibroblast-like synoviocytes (IC_{50} around 0.0028 mM).[57]

Notably, while all of these studies employed chemically synthesized parthenolide, our work demonstrates, for the first time, that PAR obtained directly from biomass through ABS extraction can achieve comparable or even superior cytotoxic effects. The observed cytotoxicity is in good agreement with the potency reported in the literature, highlighting the potential of this extraction approach to generate bioactive formulations suitable for anticancer applications in a more sustainable way.

https://doi.org/10.1021/acssuschemeng.5c10881
ACS Sustainable Chem. Eng. 2026, 14, 3370−3383

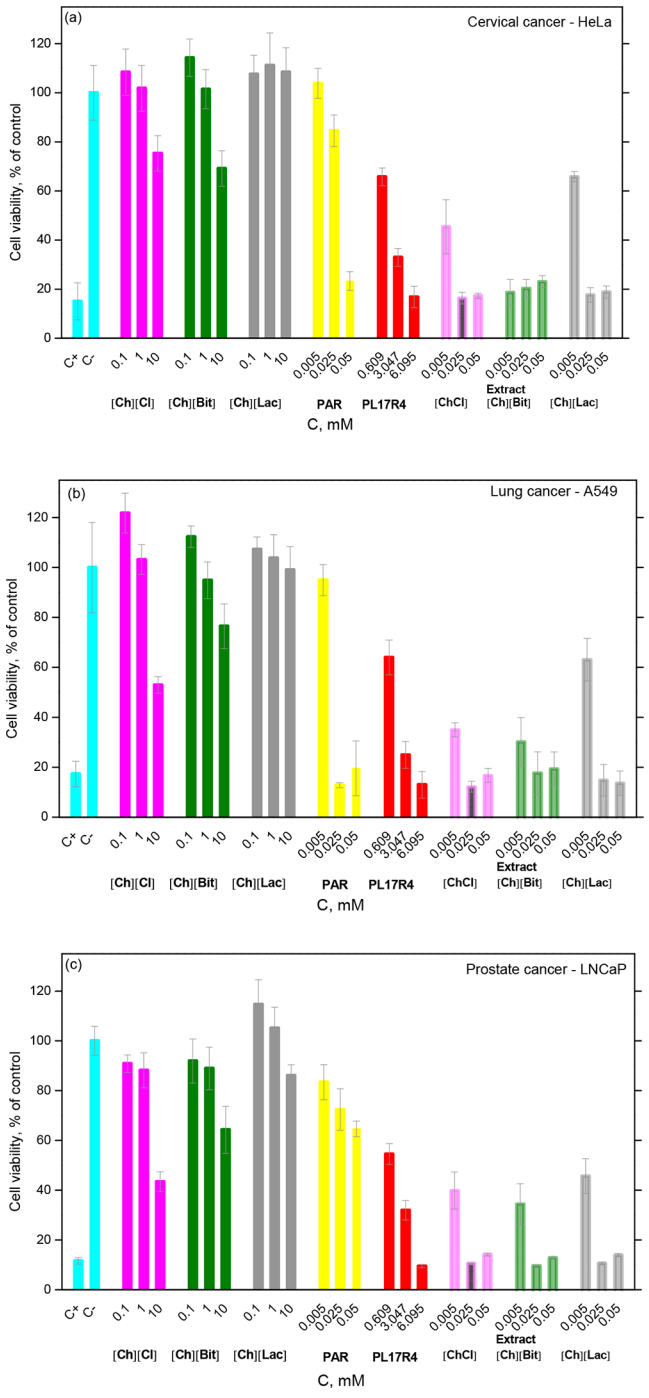

Figure 8. Cell viability (expressed relatively to the control cells) of human (a) cervical, (b) lung, and (c) prostate cancer cells, after 48 h incubation with the different extracts. Untreated cells (C−) and ethanol-treated cells (C+) were used as negative and positive controls, respectively. Values were calculated with the data obtained from three independent measurements (mean ± SD).

4. CONCLUSIONS

A thermoreversible aqueous biphasic system platform, combining Pluronic 17R4 and choline-based ionic liquids, was developed for the sustainable extraction and enrichment of parthenolide from feverfew, reducing the need for additional solvents or energy-intensive steps. The method employs monophasic extraction at mild temperatures followed by temperature-induced phase separation, thereby avoiding toxic organic solvents and minimizing energy-intensive or multistep purification procedures.

When applied to a real, complex biomass matrix, the thermoreversible ABS demonstrated high extraction efficiency, effective performance, and good selectivity. The system successfully extracts and enriches PAR from solid biomass into a directly applicable, bioactive micellar formulation, mitigating challenges associated with coextractives through the inherent selectivity of the phase-forming components and the micellization process. Moreover, preferential partitioning toward the polymer-rich phase coupled to micelle formation provides a reference value for identifying other potential polymers that could be used for similar applications.

Phase behavior studies, supported by atomistic simulations, showed that extraction performance is governed by the ionic liquid's salting-out capacity, where the anion $[DHP]^-$ proved the most effective due to its strong hydration ability, and by the dipole moment. The highest PAR yield was obtained with [Ch][Lac] (2.79 mg/g biomass), followed by [Ch][Bit]. Optimized mixing further increased extraction yields, reaching 3.52 mg/g for [Ch][Lac] and 3.42 mg/g for [Ch][Bit]. Dynamic light scattering analysis revealed micelles in the PL-rich phase with hydrodynamic diameters of 100−200 nm, which are suitable for potential drug delivery. Cytotoxicity assays demonstrated that naturally extracted PAR embedded in PL micelles exhibits higher anticancer activity than synthetic PAR.

Overall, this integrated, ecofriendly process combines extraction, enrichment, and formulation in a single step, offering a scalable route for the production of high-value bioactives and establishing a direct linking between sustainable extraction methods and biomedical applications. Additionally, this study shows the efficacy of the developed ABS platform through in vitro cytotoxicity assays. Although the Ch-ILs and PL polymer used here are generally regarded as low-toxicity materials, comprehensive in vivo pharmacokinetic and long-term toxicological studies are still required to fully assess the therapeutic potential and safety of these natural extract formulations. Future work will therefore focus on detailed ADMET evaluation to bridge the gap between this promising in vitro proof of concept and potential clinical applications. Furthermore, the general mechanism of this platform—based on hydrophobicity-driven partitioning and micellar encapsulation—suggests its high potential for the integrated production of other medium-to-high log *P* bioactives from natural sources.

■ ASSOCIATED CONTENT

Supporting Information

The Supporting Information is available free of charge at https://pubs.acs.org/doi/10.1021/acssuschemeng.5c10881.

NMR spectra 1H of ionic liquids [Ch][Lac] (Figure S1) and [Ch][Tos] (Figure S2); 3D HPLC chromatograms of pure PAR and PAR extracted from feverfew biomass in this study, recorded in the wavelength range 190−400 nm (Figure S3); optimized ion pairs of ILs investigated in this study: [Ch][Ac], [Ch][Bit], [Ch]Cl, [Ch]-[DHCit], [Ch][DHP], [Ch][Lac], and [Ch][Tos] (Figure S4); phase diagrams at 25 and 35 °C with selected extraction points for systems composed of {IL/salt + PL17R4 + H2O} (Figure S5); pH values of studied IL, ABS, and both IL- and polymer-rich phases (Table S1); weight fraction composition for binodal data

https://doi.org/10.1021/acssuschemeng.5c10881
ACS Sustainable Chem. Eng. 2026, 14, 3370−3383

for the {IL (Y) + Polymer (X) + Water} ABS at 25 °C and at p = 0.1 MPa (Tables S2a, S2b, S3a, and S3b); and weight fraction composition for binodal data for the {IL (Y) + Polymer (X) + Water} ABS (PDF)

AUTHOR INFORMATION

Corresponding Authors

Mara G. Freire − *CICECO − Aveiro Institute of Materials, Department of Chemistry, University of Aveiro, 3810-193 Aveiro, Portugal;* orcid.org/0000-0001-8895-0614; Email: maragfreire@ua.pt

Tatjana Trtić-Petrović − *Laboratory of Physics, Vinča Institute of Nuclear Sciences − National Institute of the Republic of Serbia, University of Belgrade, 11001 Belgrade, Serbia;* orcid.org/0000-0002-0817-8343; Email: ttrtic@vin.bg.ac.rs

Authors

Dajana Lazarević − *Laboratory of Physics, Vinča Institute of Nuclear Sciences − National Institute of the Republic of Serbia, University of Belgrade, 11001 Belgrade, Serbia;* orcid.org/0000-0002-5200-9512

Bojan Kopilovic − *CICECO − Aveiro Institute of Materials, Department of Chemistry, University of Aveiro, 3810-193 Aveiro, Portugal*

Sanja J. Armaković − *Department of Chemistry, Biochemistry and Environmental Protection, Faculty of Sciences, University of Novi Sad, 21000 Novi Sad, Serbia;* orcid.org/0000-0002-3665-1046

Stevan Armaković − *Department of Physics, Faculty of Sciences, University of Novi Sad, 21000 Novi Sad, Serbia*

Bruno M. Baptista − *RISE-Health, Department of Medical Sciences, Faculty of Health Sciences, University of Beira Interior, 6200-506 Covilhã, Portugal*

Fani Sousa − *RISE-Health, Department of Medical Sciences, Faculty of Health Sciences, University of Beira Interior, 6200-506 Covilhã, Portugal;* orcid.org/0000-0001-9996-2194

Slobodan B. Gadžurić − *Department of Chemistry, Biochemistry and Environmental Protection, Faculty of Sciences, University of Novi Sad, 21000 Novi Sad, Serbia;* orcid.org/0000-0002-8145-5239

Complete contact information is available at: https://pubs.acs.org/10.1021/acssuschemeng.5c10881

Notes

The authors declare no competing financial interest.

ACKNOWLEDGMENTS

This research was supported by the Science Fund of the Republic of Serbia, Grant No. 17475, Green Innovation: Unlocking the Bioactive Potential of Biomass for Enhanced Pharmaceuticals and Foods through Eco-Friendly Sustainable Technologies−VIVENDI; the Ministry of Science, Technological Development and Innovation of the Republic of Serbia (Grant Nos. 451-03-136/2025-03/200017 and 451-03-136/2025-03/200125); and the Erasmus + Programme under Key Action 1 (KA131). This work was developed within the scope of the project CICECO-Aveiro Institute of Materials, UIDB/50011/2020 (DOI 10.54499/UIDB/50011/2020), UIDP/50011/2020 (DOI 10.54499/UIDP/50011/2020), and LA/P/0006/2020 (DOI 10.54499/LA/P/0006/2020), financed by national funds through the FCT/MCTES (PIDDAC). Also, this work was a part of UBI projects UIDB/00709/2020 (DOI 10.54499/UIDB/00709/2020) and UIDP/00709/2020 (DOI 10.54499/UIDP/00709/2020), financed by national funds through the FCT/MCTES. Bruno Baptista acknowledges FCT for the Ph.D. fellowship 2023.01986.BD.

REFERENCES

(1) Bukowski, K.; Kciuk, M.; Kontek, R. Mechanisms of multidrug resistance in cancer chemotherapy. *Int. J. Mol. Sci.* **2020**, *21*, 3233.

(2) Izzo, A. A.; Stefanska, B. Natural products and cancer: From drug discovery to prevention and therapy. *Br. J. Pharmacol.* **2025**, *182*, 2069−2074.

(3) Pareek, A.; Suthar, M.; Rathore, G.; Bansal, V. Feverfew (Tanacetum parthenium L.): A systematic review. *Pharmacogn. Rev.* **2011**, *5*, 103.

(4) Liu, J.; Cui, M.; Wang, Y.; Wang, J. Trends in parthenolide research over the past two decades: A bibliometric analysis. *Heliyon* **2023**, *9*, No. e17843.

(5) Sun, J.; Li, L.; Xiong, L.; Chen, F.; She, L.; Tang, H.; et al. Parthenolide alleviates cognitive dysfunction and neurotoxicity via regulation of AMPK/GSK3β(Ser9)/Nrf2 signaling pathway. *Biomed. Pharmacother.* **2023**, *169*, 115909.

(6) Gaojian, T.; Dingfei, Q.; Linwei, L.; Xiaowei, W.; Zheng, Z.; Wei, L.; et al. Parthenolide promotes the repair of spinal cord injury by modulating M1/M2 polarization via the NF-κB and STAT1/3 signaling pathway. *Cell Death Discovery* **2020**, *6*, 97.

(7) Čretnik, L.; Škerget, M.; Knez, Z.ˇ. Separation of parthenolide from feverfew: Performance of conventional and high-pressure extraction techniques. *Sep. Purif. Technol.* **2005**, *41*, 13−20.

(8) Vicente, F. A.; Urbančič, V.; Likozar, B.; Simões, P. N.; Pereira, J. F. B. Aqueous biphasic systems as a key tool for food processing. *Curr. Opin. Food Sci.* **2023**, *50*, 100991.

(9) Dinis, T. B. V.; Valente, A. I.; Tavares, A. P. M.; Sousa, F.; Freire, M. G. Integrated platform resorting to ionic liquids comprising the extraction, purification and preservation of DNA. *Sep. Purif. Technol.* **2023**, *315*, 123646.

(10) Musarurwa, H.; Tavengwa, N. T. Stimuli-responsive polymer-based aqueous two-phase extraction of analytes in complex matrices. *J. Mol. Liq.* **2022**, *360*, 119508.

(11) Patel, N. A.; Katrak, V. K.; Ijardar, S. P. Envisioning the applicability of stimuli responsive aqueous biphasic systems in the separation technology. *J. Mol. Liq.* **2025**, *423*, 127010.

(12) Basaiahgari, A.; Gardas, R. L. Ionic liquid-based aqueous biphasic systems as sustainable extraction and separation techniques. *Curr. Opin. Green Sustainable Chem.* **2021**, *27*, 100423.

(13) Passos, H.; Luís, A.; Coutinho, J.; Freire, M. G. Thermoreversible (ionic-liquid-based) aqueous biphasic systems. *Sci. Rep.* **2016**, *6*, 20276.

(14) Kaur, G.; Kumar, H.; Singla, M. Diverse applications of ionic liquids: A comprehensive review. *J. Mol. Liq.* **2022**, *351*, 118556.

(15) Andrade, N. G.; Torquato, I. O.; Lino, N. K. B.; Pillaca-Pullo, O. S.; Veríssimo, N. V. P.; Maia, A. M. M.; et al. Aqueous biphasic systems based on Pluronics: An overview of the last 10 years. *J. Mol. Liq.* **2025**, *428*, 127530.

(16) Vargas, S. J. R.; Soares, T. S.; Sosa, F. H. B.; Hespanhol, M. C. Reverse Pluronic 10R5-based aqueous biphasic systems with ammonium salts: A novel platform for phenolic compound partitioning. *J. Chem. Eng. Data* **2025**, *70*, 3332−3343.

(17) Khaliq, N. U.; Lee, J.; Kim, S.; Sung, D.; Kim, H. Pluronic F-68 and F-127 based nanomedicines for advancing combination cancer therapy. *Pharmaceutics* **2023**, *15*, 2102.

(18) Deller, R. C.; Diamanti, P.; Morrison, G.; Reilly, J.; Ede, B. C.; Richardson, R.; et al. Functionalized triblock copolymer vectors for the treatment of acute lymphoblastic leukemia. *Mol. Pharmaceutics* **2017**, *14*, 722−732.

(19) Xu, H.; Kong, Y.; Peng, J.; Wang, W.; Li, B. Mechanism of deep eutectic solvent delignification: Insights from molecular dynamics simulations. *ACS Sustain. Chem. Eng.* **2021**, *9*, 7101−7111.

(20) Hu, X.; Zeng, Z.; Zhang, J.; Wu, D.; Li, H.; Geng, F. Molecular dynamics simulation of the interaction of food proteins with small molecules. *Food Chem.* **2023**, *405*, 134824.
(21) Thomas, R.; Mary, Y. S.; Resmi, K. S.; Narayana, B.; Sarojini, S. B. K.; Armaković, S.; et al. Synthesis and spectroscopic study of two new pyrazole derivatives with detailed computational evaluation of their reactivity and pharmaceutical potential. *J. Mol. Struct.* **2019**, *1181*, 599−612.
(22) Haruna, K.; Kumar, V. S.; Armaković, S. J.; Armaković, S.; Mary, Y. S.; Thomas, R.; et al. Spectral characterization, thermochemical studies, periodic SAPT calculations and detailed quantum mechanical profiling of 3,4-dichlorodiuron. *Spectrochim. Acta, Part A* **2020**, *228*, 117580.
(23) *Council Directive 1999/13/EC of 11 March 1999 on the limitation of emissions of volatile organic compounds due to the use of organic solvents in certain activities and installations*, Off. J. Eur. Communities: Legis. 1999, *85*, 1−22.
(24) de Souza Mesquita, L. M.; Contieri, L. S.; e Silva, F. A.; Bagini, R. H.; Bragagnolo, F. S.; Strieder, M. M.; Sosa, F. H. B.; Schaeffer, N.; Freire, M. G.; Ventura, S. P. M.; et al. Path2Green: Introducing 12 green extraction principles and a novel metric for assessing sustainability in biomass valorization. *Green Chem.* **2024**, *26*, 10087−10106.
(25) Sun, L.; Yuan, W.; Wen, G.; Yu, B.; Xu, F.; Gan, X.; et al. Parthenolide inhibits human lung cancer cell growth by modulating the IGF-1R/PI3K/Akt signaling pathway. *Oncol. Rep.* **2020**, *44*, 1184−1193.
(26) Bannwarth, C.; Caldeweyher, E.; Ehlert, S.; Hansen, A.; Pracht, P.; Seibert, J.; et al. Extended tight-binding quantum chemistry methods. *Wiley Interdiscip. Rev.: Comput. Mol. Sci.* **2021**, *11*, No. e1493.
(27) Bannwarth, C.; Ehlert, S.; Grimme, S. GFN2-xTB—An accurate and broadly parametrized self-consistent tight-binding quantum chemical method with multipole electrostatics and density-dependent dispersion contributions. *J. Chem. Theory Comput.* **2019**, *15*, 1652−1671.
(28) Armaković, S.; Armaković, S. J. Atomistica.online − web application for generating input files for ORCA molecular modelling package made with the Anvil platform. *Mol. Simul.* **2023**, *49*, 117−123.
(29) Armaković, S.; Armaković, S. J. Online and desktop graphical user interfaces for xtb programme from atomistica.online platform. *Mol. Simul.* **2024**, *50*, 560−570.
(30) Wales, D. J.; Doye, J. P. K. Global optimization by basin-hopping and the lowest energy structures of Lennard-Jones clusters containing up to 110 atoms. *J. Phys. Chem. A* **1997**, *101*, 5111−5116.
(31) Goedecker, S. Minima hopping: An efficient search method for the global minimum of the potential energy surface of complex molecular systems. *J. Chem. Phys.* **2004**, *120*, 9911−9917.
(32) Grimme, S.; Hansen, A.; Ehlert, S.; Mewes, J.-M. r2SCAN-3c: A "Swiss army knife" composite electronic-structure method. *J. Chem. Phys.* **2021**, *154*, 064103.
(33) Caldeweyher, E.; Mewes, J.-M.; Ehlert, S.; Grimme, S. Extension and evaluation of the D4 London-dispersion model for periodic systems. *Phys. Chem. Chem. Phys.* **2020**, *22*, 8499−8512.
(34) Caldeweyher, E.; Ehlert, S.; Hansen, A.; Neugebauer, H.; Spicher, S.; Bannwarth, C.; et al. A generally applicable atomic-charge dependent London dispersion correction. *J. Chem. Phys.* **2019**, *150*, 154122.
(35) Helmich-Paris, B.; de Souza, B.; Neese, F.; Izsák, R. An improved chain of spheres for exchange algorithm. *J. Chem. Phys.* **2021**, *155*, 104109.
(36) Neese, F. An improvement of the resolution of the identity approximation for the formation of the Coulomb matrix. *J. Comput. Chem.* **2003**, *24*, 1740−1747.
(37) Neese, F.; Wennmohs, F.; Hansen, A. U.; Becker, U. Becker, Efficient, approximate and parallel Hartree−Fock and hybrid DFT calculations: A 'chain-of-spheres' algorithm for the Hartree−Fock exchange. *Chem. Phys.* **2009**, *356*, 98−109.
(38) Neese, F.; Wennmohs, F.; Becker, U.; Riplinger, C. The ORCA quantum chemistry program package. *J. Chem. Phys.* **2020**, *152*, L224108.
(39) Neese, F. The SHARK integral generation and digestion system. *J. Comput. Chem.* **2022**, *44*, 381−396.
(40) Neese, F. Software update: The ORCA program system, version 4.0. *Wiley Interdiscip. Rev.: Comput. Mol. Sci.* **2018**, *8*, No. e1327.
(41) Neese, F. The ORCA program system. *Wiley Interdiscip. Rev.: Comput. Mol. Sci.* **2012**, *2*, 73−78.
(42) *SchröDinger Release 2022−1*; Maestro, Schrödinger, LLC, New York, NY, 2022.
(43) Jorgensen, W. L.; Tirado-Rives, J. The OPLS [optimized potentials for liquid simulations] potential functions for proteins, energy minimizations for crystals of cyclic peptides and crambin. *J. Am. Chem. Soc.* **1988**, *110*, 1657−1666.
(44) Jorgensen, W. L.; Maxwell, D. S.; Tirado-Rives, J. Development and testing of the OPLS all-atom force field on conformational energetics and properties of organic liquids. *J. Am. Chem. Soc.* **1996**, *118*, 11225−11236.
(45) Shivakumar, D.; Williams, J.; Wu, Y.; Damm, W.; Shelley, J.; Sherman, W. Prediction of absolute solvation free energies using molecular dynamics free energy perturbation and the OPLS force field. *J. Chem. Theory Comput.* **2010**, *6*, 1509−1519.
(46) Harder, E.; Damm, W.; Maple, J.; Wu, C.; Reboul, M.; Xiang, J. Y.; et al. OPLS3: A force field providing broad coverage of drug-like small molecules and proteins. *J. Chem. Theory Comput.* **2016**, *12*, 281−296.
(47) Roos, K.; Wu, C.; Damm, W.; Reboul, M.; Stevenson, J. M.; Lu, C.; et al. OPLS3e: Extending force field coverage for drug-like small molecules. *J. Chem. Theory Comput.* **2019**, *15*, 1863−1874.
(48) Lazarević, D.; Mušović, J.; Trtić-Petrović, T.; Gadžurić, S. Partition of parthenolide in ternary {block copolymer + biocompatible ionic liquid or natural deep eutectic solvent + water} systems. *Sep. Purif. Technol.* **2023**, *314*, 123653.
(49) Parthenolide; PubChem, https://pubchem.ncbi.nlm.nih.gov/compound/Parthenolide.
(50) Dimitrijević, A.; Tavares, A. P. M.; Almeida, M. R.; Vraneš, M.; Sousa, A. C. A.; Cristóvão, A. C.; Trtić-Petrović, T.; Gadžurić, S.; Freire, M. G. Valorization of Expired Energy Drinks by Designed and Integrated Ionic Liquid-Based Aqueous Biphasic Systems. *ACS Sustainable Chem. Eng.* **2020**, *8*, 5683−5692.
(51) Herrera, F.; Martin, V.; Rodriguez-Blanco, J.; García-Santos, G.; Antolín, I.; Rodriguez, C. Intracellular redox state regulation by parthenolide. *Biochem. Biophys. Res. Commun.* **2005**, *332*, 321−325.
(52) Marete, E. N.; Jacquier, J. C.; O'Riordan, D. Effects of extraction temperature on the phenolic and parthenolide contents, and colour of aqueous feverfew (Tanacetum parthenium) extracts. *Food Chem.* **2009**, *117*, 226−231.
(53) Marete, E. N.; Jacquier, J.-C.; O'Riordan, D. Feverfew as a source of bioactives for functional foods: Storage stability in model beverages. *J. Funct. Foods* **2011**, *3*, 38−43.
(54) Torchilin, V. P. Structure and design of polymeric surfactant-based drug delivery systems. *J. Controlled Release* **2001**, *73*, 137−172.
(55) Ejigah, V.; Owoseni, O.; Bataille-Backer, P.; Ogundipe, O. D.; Fisusi, F. A.; Adesina, S. K. Approaches to Improve Macromolecule and Nanoparticle Accumulation in the Tumor Microenvironment by the Enhanced Permeability and Retention Effect. *Polymers* **2022**, *14*, 2601.
(56) Dey, S.; Murmu, N.; Mukherjee, R.; Mondal, A.; Mondal, T.; Haldar, S.; Molla, M. R.; Murmu, N.; Giri, B. Parthenolide-loaded stimuli-responsive cross-linked nanocarrier for targeting and killing triple-negative breast cancer cells. *ACS Appl. Nano Mater.* **2024**, *7*, 12944−12957.
(57) Parada-Turska, J.; Mitura, A.; Brzana, W.; Jabłoński, M.; Majdan, M.; Rzeski, W. Parthenolide inhibits proliferation of fibroblast-like synoviocytes in vitro. *Inflammation* **2008**, *31*, 281−285.

https://doi.org/10.1021/acssuschemeng.5c10881
ACS Sustainable Chem. Eng. 2026, 14, 3370−3383